

Task Parameter Extrapolation via Learning Inverse Tasks from Forward Demonstrations

Serdar Bahar¹, Fatih Dogangun¹, Matteo Saveriano², Yukie Nagai³, Emre Ugur¹

Abstract—Generalizing skill policies to novel conditions remains a key challenge in robot learning. Imitation learning methods, while data-efficient, are largely confined to the training region and consistently fail on input data outside it, leading to unpredictable policy failures. Alternatively, transfer learning approaches offer methods for trajectory generation robust to both changes in environment or tasks, but they remain data-hungry and lack accuracy in zero-shot generalization. We address these challenges by framing the problem in the context of task inversion learning and proposing a novel joint learning approach to achieve accurate and efficient knowledge transfer. Our method constructs a common representation of the forward and inverse tasks, and leverages auxiliary forward demonstrations from novel configurations to successfully execute the corresponding inverse tasks, without any direct supervision. We show the extrapolation capabilities of our framework via ablation studies and experiments in simulated and real-world environments that require complex manipulation skills with a diverse set of objects and tools, where we outperform diffusion-based alternatives.

Index Terms—Learning from Demonstration, Representation Learning, Transfer Learning, Joint Learning, Skill Generalization

I. INTRODUCTION

A fundamental challenge in robotics is developing methods for efficient, generalizable skill acquisition. An autonomous robot is expected to adapt to variations in its environment as well as changes in task or skill specifications. This requires skill policies that can generalize beyond the specific conditions seen during training, a capability that still remains a significant obstacle for many current learning paradigms.

Data-driven approaches in robotics have demonstrated impressive generalization capabilities, but often at the cost of extensive data collection and interaction with the environment [1]–[3]. Transfer learning frameworks aim to mitigate this by leveraging knowledge across tasks. A common technique, domain randomization, focuses on creating policies that are robust to variations in the environment, such as changes in lighting, friction, or object textures [1], [4], [5]. However, these approaches are mostly designed to handle environmental changes within a single task definition. While other methods, such as cross-domain transfer, exist, they often require additional training in the target domain and struggle with data efficiency and robust zero-shot performance [6], [7].

Imitation learning (IL) offers a more data-efficient alternative by leveraging expert demonstrations for the task of interest. Foundational approaches in this domain include Dynamic Movement Primitives (DMPs) [8], [9], which use systems of

differential equations and Probabilistic Movement Primitives (ProMPs) [10], which model a distribution over trajectories. Deep learning has given rise to powerful and flexible methods such as Conditional Neural Movement Primitives (CNMPs) [11] and Stable Movement Primitives (StableMP) [12], which leverage neural networks to learn complex, non-linear skills directly from demonstration data. More recently, advancements in deep generative modeling have enabled robotic policies to represent rich distributions using diffusion-based and flow-based models [13]–[16]. Although these methods are considered highly effective, their operational strength lies in *interpolation*, allowing them to accurately generate behaviors similar to the expert demonstrations provided, but they consistently fail at *extrapolation* [17]. This inability to generalize beyond the training data results in unpredictable trajectories for novel inputs, often compromising the success of downstream tasks that rely on the trained policy. While some recent work has shown promise in learning explicit mathematical relationships to enable extrapolation [18], the problem remains largely unsolved for mainstream IL frameworks.

We explore the paradigm of joint learning as a mechanism for zero-shot extrapolation, specifically within the structured domain of **task inversion**. Many robotic skills naturally exist as forward-inverse pairs (e.g., pushing an object to a goal and pulling it back; assembling a mechanical component and disassembling it for repair). We observe that if a common representation of forward and inverse tasks is obtained, an inverse task for a novel environment configuration can be generalized only from a provided forward task for a similar environment configuration (e.g., learning to disassemble a component by observing its assembly). Following this main idea, we propose a novel joint learning framework that effectively transfers knowledge from a forward task to its inverse counterpart by learning a common representation for both. Specifically, excluding out-of-distribution action generation from our scope, we focus on inferring inverse executions that are similar to an observed set of sensorimotor demonstrations. For instance, a robot, which acquired pushing and pulling skills for a set of objects, can utilize our framework to infer how to pull a novel object after observing how the object is pushed. Our framework can effectively scale to a wide range of objects and tools that share complex, underlying manipulation strategies.

To achieve this, our method extends the framework of Conditional Neural Processes (CNP) [19] and Deep Modality Blending Networks (DMBN) [20]. CNP [19] is a meta-learning network that model complex data distributions through a Gaussian process-based perspective and has proven instrumental for skill learning in the robotic domain [11], [20]–[22]. In particular, DMBN [20] is a multi-modal architecture

This work has been supported by the *INVERSE* project (no. 101136067), funded by the EU.

¹Bogazici University ²University of Trento ³The University of Tokyo

that jointly learns different modalities of robot actions with CNP by forming a shared latent space of multi-modal observations. Our contributions include:

- 1) A joint learning framework that enables zero-shot extrapolation to novel task parameters for an *inverse task* by leveraging auxiliary demonstrations from its corresponding *forward task*.
- 2) A complete training methodology, including a demonstration matching algorithm based on initial and final environment states and an interleaved training schedule, that allows a flexible data demonstration process and efficient learning from datasets including auxiliary demonstrations.
- 3) Separating task parameter conditioning from sensorimotor encoding, which is crucial for generalizing to unseen parameters.

We extensively evaluate our proposed method through varying settings. First, we conducted a synthetic trajectory experiment showing the necessity of pairing forward and inverse demonstrations. Then, we performed a simulation experiment with a rich set of objects, demonstrating the superior extrapolation capabilities of our method compared to diffusion-based alternatives (inspired by Chi et al. [13]). Lastly, we showed the feasibility of our method on real-world skills, where extrapolation is required when operating with tools.

II. METHOD

We are given a demonstration set that includes forward executions of skills and their inverse counterparts, along with their task parameters, where forward and inverse demonstrations are not necessarily matched, and not all counterparts are observed. Inverse executions represent executions that induce the opposite state transition in the environment. Our aim is to infer and generate inverse executions for novel task parameters by leveraging auxiliary forward demonstrations available for those parameters. The executions may or may not be direct reversals of the forward sensorimotor trajectories, depending on the complexity of the task. In this section, we first briefly introduce Conditional Neural Processes and Deep Modality Blending Networks, the frameworks on which our system is built. We then provide the problem formulation and a general overview of our framework, and finally present the details of our skill training and generalization methods.

A. Background

1) *Conditional Neural Processes (CNP)*: Given a set of input data, CNP [19] estimates a Gaussian process conditioned on a varying number of permutationally invariant input observations. To achieve this, CNP employs a shared parameter encoder network, E_ϕ , to encode observations into a fixed-size representation, r , and a decoder network, Q_θ , which produces Gaussian distributions conditioned on r with input x_q . CNP computation can be expressed as

$$\mu_q, \sigma_q = Q_\theta(x_q \oplus \frac{\sum_{i=1}^n E_\phi(x_i, y_i)}{n}) \quad (1)$$

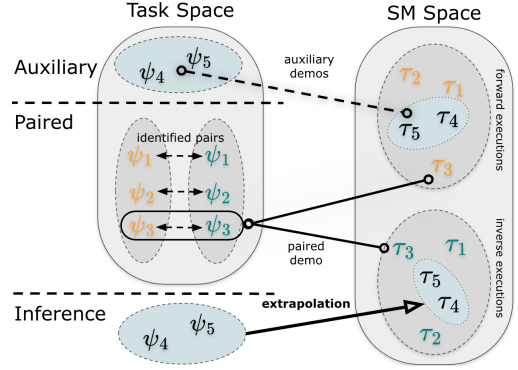


Fig. 1. The demonstrations are decoupled into task and sensorimotor (SM) spaces. In the top, demonstrations are visualized as lines between task parameters (ψ) and SM executions (τ). Our method will first identify correspondence between demonstrations and learns a common representation of the forward and inverse tasks using paired and auxiliary datasets. The learning objective is to infer inverse executions for task parameters drawn from the auxiliary distribution.

where μ_q and σ_q are the mean and standard deviation of the predicted Gaussian distribution, respectively, \oplus is the concatenation operator, and $\{(x_i, y_i)\}_{i=1}^n$ are input observations to the network. CNP can be trained using maximum likelihood, producing robust predictions inside the input observation space.

2) *Deep Modality Blending Networks (DMBN)*: DMBN [20] was proposed as a neural action recognition mechanism inspired by the mirror neuron system [23], where the robot's motor patterns were automatically triggered by observing the corresponding actions executed by itself or other robots. For this, the robot jointly learns an action across different modalities, such as joint angles and image sequences, and employs multiple encoder and decoder networks, each accounting for a different modality of data. The training and inference of DMBN are similar to those of CNP, except that an aggregation operation across modalities is used. DMBN can be conditioned on any desired image at any time step, and can generate a motor trajectory consistent with the desired conditioning in parallel, avoiding the accumulation of prediction errors.

B. Problem Definition

Formally, we define a forward task as one that causes a state transition from S_{init} to S_{final} , and its corresponding inverse task as one that reverses this transition, from S_{final} to S_{init} . The demonstrations are defined by a tuple that includes S_{init} and S_{final} , the sensorimotor trajectory (τ) observed during this transition, and the corresponding task parameter (ψ), which might be a scalar value or an image, depending on the task. The initial unorganized sets of forward and inverse demonstrations are denoted by $\mathcal{D}_F = \{(\tau_i^F, \psi_i^F, S_i^{F,init}, S_i^{F,final})\}_{i=1}^N$ and $\mathcal{D}_I = \{(\tau_i^I, \psi_i^I, S_i^{I,init}, S_i^{I,final})\}_{i=1}^N$, respectively. Furthermore, the dataset for the forward task is augmented with an auxiliary set of M additional demonstrations, denoted as $\mathcal{D}_{aux}^F = \{(\tau_j^F, \psi_j^F, S_j^{F,init}, S_j^{F,final})\}_{j=N+1}^{N+M}$. The objective is to infer inverse task executions for task parameters drawn from the same distribution as those in \mathcal{D}_{aux}^F .

The details of the target problem is illustrated in Figure 1. Our system is trained with forward-inverse pairs of task parameters and sensorimotor (SM) trajectories (numbered 1-3 in the figure), and auxiliary forward-only out-of-distribution task parameters and in-distribution SM trajectories (numbered 3-4 in the upper part of the figure). We address the task extrapolation problem by inferring the SM trajectories of inverse tasks for out-of-distribution task parameters, i.e., novel task parameters that were not provided in the inverse demonstrations. As shown in the figure on the right, with blue ellipses, we expect the queried task parameters to be in-distribution with auxiliary task parameters and SM trajectories to be within the distribution of the demonstrated SM space.

C. Method Overview

Our method proceeds in two stages. In the first stage, a paired demonstration dataset is constructed by identifying forward and inverse demonstrations that are counterparts. Such pairings are crucial, as the common representation relies on explicit correspondences to capture the relationships between task parameters and their forward and inverse executions. The resulting dataset of paired forward and inverse demonstrations (\mathcal{D}_{paired}) is illustrated with dashed lines in Figure 1. In the second stage, skill training operates on this paired dataset and the auxiliary forward dataset. The training requires (1) separate encoding of the task parameter to avoid failures on novel task parameters at inference time, and (2) joint training over both the paired and auxiliary demonstrations to form a common latent representation while enriching it with auxiliary information. With these two conditions, the trained model can infer inverse executions for task parameters drawn from the auxiliary distribution, as illustrated at the bottom of Figure 1.

D. Identifying Forward-Inverse Pairs

Given the unorganized sets of forward (\mathcal{D}_F) and inverse (\mathcal{D}_I) demonstrations, this section describes how the forward-inverse pairs are identified, and the paired dataset (\mathcal{D}_{paired}) is formed. Establishing forward-inverse execution correspondences in the unorganized sets of forward and inverse demonstrations can be formulated as a linear sum assignment problem. Given the two initial demonstration sets, \mathcal{D}_F and \mathcal{D}_I , we construct a cost matrix $C \in \mathbb{R}^{N \times N}$ where each entry C_{ij} quantifies the dissimilarity between the final environment state of the i -th forward demonstration and the initial environment state of the j -th inverse demonstration. The optimal bijective pairing is then obtained by minimizing the total assignment cost. In our experiments, where the environment is represented as state-based vectors, we use Euclidean distance as the dissimilarity measure. Scenarios involving higher-dimensional environment representations, such as images, would require a more specific similarity metric. Note that the auxiliary set \mathcal{D}_{aux} is excluded from this process. The problem can be solved using the Hungarian algorithm [24], and the resulting bijection is used to create a paired dataset for joint learning.

E. Skill Training for Task Parameter Extrapolation

Training with paired forward-inverse trajectories is illustrated in the upper row of Figure 2. For training, first,

Training

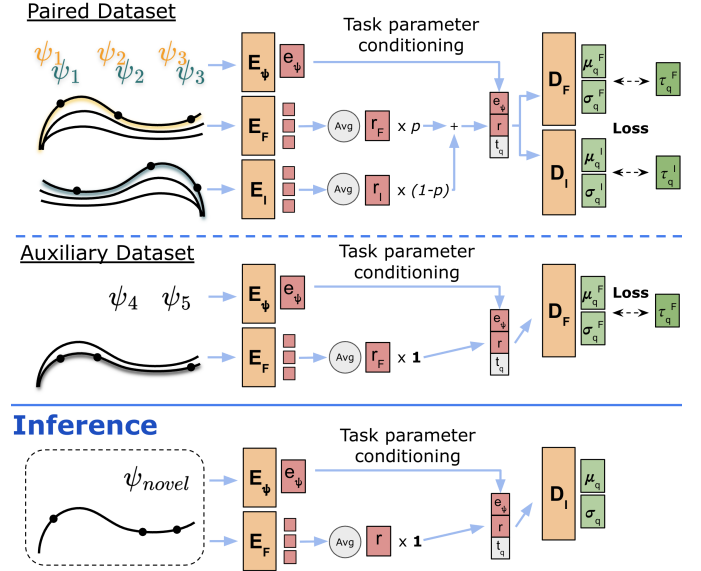


Fig. 2. Overview of the proposed method. The first and second rows show the overall paired and auxiliary passes, respectively, during training. The third row shows the inference conditioned on the novel task parameter and observations from a forward execution to generate the full inverse execution.

a pair of forward-inverse demonstrations (τ^F and τ^I) is randomly chosen from the dataset. Then, random observation points (empirically set to range from 1 to 15) are selected from the forward and inverse demonstrations in the pair. These observations (shown with 3 dots in the figure) are independently sampled with time-steps normalized to a $[0, 1]$ time scale. Next, these observations are processed by separate forward and inverse encoders (E_F and E_I), and outputs are averaged to yield representations for the pair (r_F and r_I). These representations are aggregated into a unified representation (r) via a convex combination with a stochastic weight: $r = p \times r_F + (1 - p) \times r_I$, where $0 \leq p \leq 1$, as shown in Figure 2. A separate module (E_ψ) is employed to embed the task parameter (ψ), where the embedding (e_ψ) is generated by a fully connected neural network for vector inputs and by a convolutional neural network for image inputs. This embedding (e_ψ) is concatenated with the common latent representation (r) and a randomly chosen query time step, and then passed through both forward and inverse decoders (D_F and D_I) to predict sensorimotor values for the corresponding time step, as shown on the right side of the upper row in Figure 2. The forward and inverse decoders generate the mean and standard deviation of a normal distribution, and the network is optimized by back-propagating the negative log-likelihood of the predicted sensorimotor values against the ground truth at that specific time step. This procedure is repeated with random forward-inverse demonstration pairs and with random observations from these pairs until convergence. After training, we expect our system to generate the full inverse sensorimotor trajectory from sampled points of a chosen forward trajectory by setting $p = 1$ and by querying the system with all time points from 0 to 1.

Training with auxiliary forward trajectories whose inverse counterparts are missing is shown in the second row of Figure 2. To incorporate auxiliary data into training, we employ an interleaved training scheme with two types of forward passes. In the **paired pass**, a batch of trajectory pairs is sampled from the paired dataset (\mathcal{D}_{paired}), and the common latent representation is formed by a random convex combination. In the **auxiliary pass**, a batch is sampled from the auxiliary dataset (\mathcal{D}_{aux}), and the common latent representation is derived solely from the sensorimotor observations of the forward task, with the combination weight (p) fixed to 1, as shown in the second row in the figure. The parameters of the inverse encoder and decoder (E_I and D_I) remain frozen during the auxiliary pass. Note that the auxiliary pass is aimed to integrate out-of-distribution task parameters into the common latent space and the representation capacities of the forward encoder and decoder (E_F and D_F) stay the same as we expect in-distribution sensorimotor executions from these task parameters. During training, two forward passes are alternated stochastically (auxiliary pass executed with probability p_{aux}) to balance learning sensorimotor executions with paired task parameters and incorporating novel task parameters (and their unpaired forward executions) into the common latent space. We determined the auxiliary pass probability (p_{aux}) empirically during our evaluations.

Inference of inverse trajectories for novel parameters is shown in the bottom row of Figure 2. Here, our aim is to generate the trajectory of a novel inverse task by querying our system with the novel task parameter and observation points from its forward execution. As shown in the figure, these observations are processed by E_F and then averaged to generate the common representation (r), which can be used to generate both forward and inverse sensorimotor trajectories. Next, r is used as input to D_I , along with the task parameters, to generate the complete inverse sensorimotor trajectory by querying the system at all time steps from 0 to 1.

III. EXPERIMENTS

To evaluate the core contributions of the proposed method, we conducted experiments with synthetic data, simulations, and real-robot executions, and compared it with diffusion-based joint learning alternatives, demonstrating its advantages.

A. Synthetic Data

We designed a synthetic scenario to systematically analyze the importance of identifying forward-inverse correspondence in unorganized sets of forward and inverse demonstrations during skill training. In particular, we focused on the effect of correspondence quality on skill training performance with paired demonstrations, as it is directly impacted by the learned shared representation, which in turn affects task parameter extrapolation. To this end, we abstract away other complexities by modeling sensorimotor executions as explicit mathematical expressions, their inverse counterparts as time-reversed trajectories, and task parameters and environment states as quantities derived from these expressions.

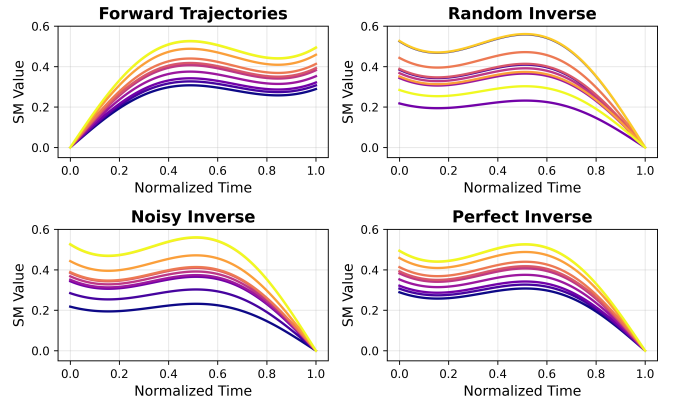


Fig. 3. Visualization of the synthetic trajectory datasets. The color correspondence illustrates the pairing. The trajectories for the forward task is on the upper left. Remain plots show the corresponding inverse task trajectories under different conditions: randomly paired (**Random**), paired using our algorithm with noisy task parameters (**Noisy**), and perfectly paired (**Perfect**).

1) *Experiment Setup*: The datasets consist of trajectories that are sinusoidal curves defined over a normalized time period $[0, 1]$. For the forward task, we define the trajectory as $\tau_F(t) = \psi \cdot \sin(\frac{3}{2}\pi t) + t$, and we use its time reversal, $\tau_I(t) = \tau_F(1 - t)$, representing the inverse task, where task parameter (ψ) is the scalar amplitude ranging between 0.1 and 0.25. Also, for a trajectory τ , the environment states (S_{init} and S_{final}) are $\tau(0)$ and $\tau(1)$, respectively.

a) *Datasets*: To evaluate our matching algorithm, we created four training conditions based on how the initial demonstration sets \mathcal{D}_F and \mathcal{D}_I were formed and paired. The demonstration sets are visualized in Figure 3.

- **Random**: Demonstrations in \mathcal{D}_F and \mathcal{D}_I were generated from randomly sampled amplitudes, and randomly paired.
- **Paired Noisy**: Demonstrations in \mathcal{D}_F and \mathcal{D}_I were generated from randomly sampled amplitudes, and paired using our proposed algorithm.
- **Paired Perfect**: Demonstrations in \mathcal{D}_F were generated as in the previous conditions. Inverse task trajectories with the *same* amplitudes were used to form \mathcal{D}_I .
- **Uniform**: Demonstrations in \mathcal{D}_F were generated from uniformly spaced amplitudes, and their perfectly corresponding trajectories were used to create \mathcal{D}_I , mimicking ideally collected and perfectly paired demonstrations.

b) *Model*: The model uses an MLP-based encoder and decoder with 170K trainable parameters, trained on five different datasets per condition for 60K steps with a batch size of 4 using the AdamW optimizer (lr: 5×10^{-4} , weight decay: 1×10^{-3}). We generated trajectories for the forward task from 20 novel test amplitudes, conditioned the model on observations, and queried it to generate the corresponding trajectory for the inverse task. To assess the model's performance, we used the Mean Squared Error (MSE) between the generated and ground-truth inverse task trajectories.

2) *Results*: The model trained on the **Random** dataset performed the worst with an MSE of 8.87 ± 14.3 (in units of 10^{-3}), while applying our matching algorithm (**Paired Noisy**) yielded a statistically significant improvement (paired t-test,

$p < 0.001$), reducing the MSE by over 80% to 1.22 ± 1.48 (in units of 10^{-3}) and demonstrating that establishing a correct correspondence is critical for learning the shared structure and generating trajectories. The models trained on the idealized datasets, **Paired Perfect** and **Uniform**, achieved significantly lower errors (approximately 14 and 140 times lower, respectively) than in the **Paired Noisy** condition (paired t-test, $p < 0.001$). These results conclusively suggest that structured demonstration pairing is not only beneficial but also a fundamental requirement for joint learning of tasks. Besides pairing, ideally collected and paired demonstrations also help the model to generate more accurate trajectories.

B. Object Extrapolation in Robot Simulation

We designed an experiment in a simulated robotic manipulation environment to evaluate the proposed method as a whole. In particular, we assessed the model’s ability to extrapolate learned manipulation skills to entirely novel objects, given paired demonstrations for two object categories (horizontal and vertical cylinders) and forward-only demonstrations for the test object categories (spheres and boxes). For instance, given only a top-down view of a novel box, the model must infer the correct manipulation strategy to pull the box across the table (an inverse task) and execute it by reasoning about the box’s position and orientation. Crucially, the model has never observed a pull demonstration involving a box and relies solely on a handful of forward demonstrations of boxes with varying sizes, positions, and orientations, along with other paired demonstrations for various objects. We also examined the role of the matching algorithm in both perfect and noisy data-collection scenarios and compared the proposed method against three Diffusion Policy-inspired [13] joint learning alternatives.

1) *Experiment Setup*: The experimental environment consists of a 7-DoF *xArm 7* robotic arm with a gripper simulated in the MuJoCo [25] physics engine. We define two related object manipulation tasks on a tabletop: **forward task**, manipulating an object from a designated start area to an end area of the table, and **inverse task**, manipulating the object in the reverse direction, which require distinct manipulation strategies due to the asymmetry in the robot’s workspace. Visualization of demonstrations for the designated forward-inverse tasks are shown in Figure 5. The required robot action is determined by the object’s physical properties, following the

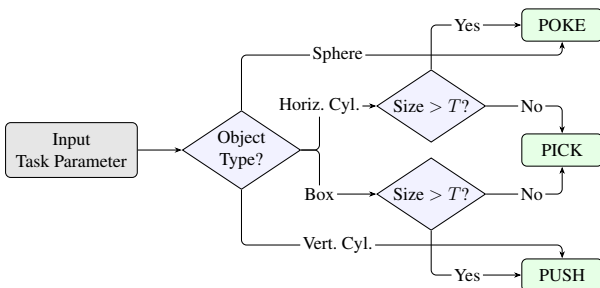


Fig. 4. Task controller logic. The flowchart illustrates the underlying decision process in provided demonstrations.

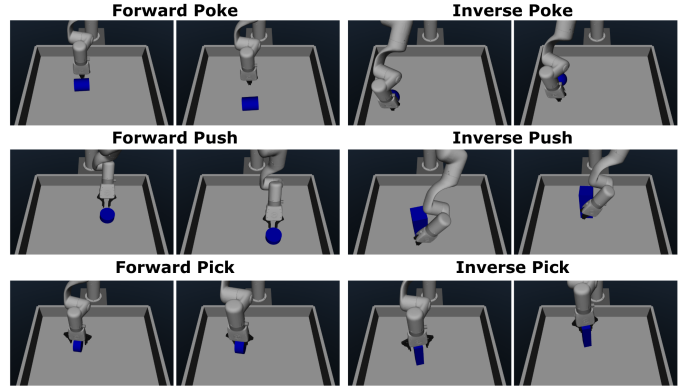


Fig. 5. Visualization of the manipulation tasks in the simulated environment. The figure shows example executions for the designated forward task (moving an object to a target) and its inverse task with three different modalities for various object categories (left to right, top to bottom: large horizontal cylinder, sphere, vertical cylinder, large box, small horizontal cylinder, small box).

logic outlined in Figure 4. The set of objects comprises vertical cylinders, horizontal cylinders, spheres, and boxes of varying sizes and orientations. The task parameter (ψ) is defined by a top-down depth image of the object and its initial position on the table. Lastly, the initial and final states (S_{init} and S_{final}) include the object depth image and the position of the object.

a) *Datasets*: To investigate the robustness of our pairing algorithm, we created the following datasets using joint angle measurements of the simulated robot:

- **Perfect Initial** ($\mathcal{D}_F^{\text{Perfect}}, \mathcal{D}_I^{\text{Perfect}}$): 60 demonstration pairs (20 for each action type) where all objects are **cylinders** and the task parameters for the forward and the inverse demonstrations are identical, leading to synchronized final and initial states for forward-inverse demonstrations, representing a perfect data collection scenario.
- **Noisy Initial** ($\mathcal{D}_F^{\text{Noisy}}, \mathcal{D}_I^{\text{Noisy}}$): 60 demonstration pairs with **identical objects**, Y-positions for demonstration for the tasks sampled independently, representing a noisy data collection scenario.
- **Auxiliary** (\mathcal{D}_{aux}): 20 demonstrations of Task A, including randomly generated 4 spheres, 8 large boxes and 8 small boxes with randomly sampled Y-positions.

b) *Compared Models*: We compared the proposed method with three DP-inspired approaches; specifically, in the Paired Perfect case. The compared models are listed below:

- **Ours**: Proposed method with MLPs as encoders and decoders.
- **DP-Dual**: DP-based alternative for the proposed method. Two CNN-based decoders predicting forward and inverse joint angles with shared, global conditioning on the state information. Actions represented as joint angles in single timestep, state information represented as action timestep and task parameter.
- **DP-2Head**: Single CNN-based decoder. Actions represented as concatenation of forward and inverse joint angles in single timestep, state information represented as action timestep and task parameter.
- **DP-Mode**: Single CNN-based decoder. Actions represented as either forward or inverse joint angles in single

TABLE I
SUCCESS RATES (MEAN \pm STD) IN INVERSE TASK OUT OF 10 TRIALS
OVER 5 RUNS FOR SIMULATION EXPERIMENT

	Poke	Push	Pick
Paired Perfect	10.0 \pm 0.0	8.6 \pm 0.55	8.2 \pm 1.48
Paired Noisy	10.0 \pm 0.0	6.4 \pm 0.55	6.8 \pm 1.92
Unpaired Perfect	0.0 \pm 0.0	0.0 \pm 0.0	3.4 \pm 1.14
Unpaired Noisy	0.4 \pm 0.55	2.0 \pm 2.0	0.0 \pm 0.0

timestep, state information represented as action timestep, task parameter and modality bit (forward or inverse). Note that since forward and inverse action steps correspond to different data points, the pairing of forward and inverse demonstrations are irrelevant to this model.

The task parameter dimensionality is reduced to 75 by extracting features from a pre-trained ResNet50 [26] and applying Principal Component Analysis. For statistical validity, we generated five unique versions of Perfect and Noisy Initial datasets and used the same Auxiliary dataset along with them. To also test the efficacy of our matching algorithm, we created a total of four training conditions for our model, including datasets paired according to our matching algorithm, and randomly paired datasets. The models for the proposed method (940K trainable weights) are trained with $p_{\text{aux}} = 0.20$, batch size 24, for 80K steps using AdamW optimizer (lr: $5 * 10^{-4}$, weight decay: $1 * 10^{-3}$). The baselines DP-Dual (135M parameters), DP-2Head, and DP-Mode (67M parameters each) are trained with horizon 64, 8 predicted actions, batch size 256, for 200K steps with AdamW optimizer (lr: $5 * 10^{-4}$, weight decay: $1 * 10^{-6}$). DP-based baselines were developed and tuned using the LeRobot library [27].

2) *Results*: We evaluated the trained policies on a test set composed of 10 spheres, 10 large boxes, and 10 small boxes that were entirely novel and not present in any training or auxiliary data. Inverse task trajectories are generated according to the determined task parameters, and their performance was measured by task success rate, trajectory, and final object position error based on the ground truth inverse task trajectory of the controller logic described in Figure 4.

a) *Effect of Matching Algorithm*: The efficacy of our pairing algorithm is demonstrated by the task success rates. As shown in Table I, models trained using our algorithm on both *Perfect* and *Noisy* initial datasets achieved high success rates across all interaction modalities. In contrast, models trained with randomly paired demonstrations exhibited near-total failure. This result once again demonstrates that a meaningful correspondence between demonstration is a fundamental prerequisite for our method.

The trajectory and object errors are provided in Table II and Figure 6, respectively. For the pick modality, which represents the most complex manipulation skill for our setup, due to the need for precise gripper position and orientation alignment, the model trained on the *Perfect* dataset produced trajectories with significantly lower error (paired t-test, $p < 0.001$) and achieved a more accurate final object placement (paired t-test, $p < 0.05$). This might suggest that high-precision skills are more sensitive to the quality of the demonstration pairs.

TABLE II
RMSE FROM GROUND TRUTH (MEAN \pm STD) OVER 5 RUNS IN DEGREES.

	Poke	Push	Pick
Paired Perfect	2.772 \pm 2.010	9.719 \pm 8.181	2.846 \pm 2.196
Paired Noisy	2.481 \pm 1.546	9.474 \pm 6.981	3.921 \pm 2.444
Unpaired Perfect	36.70 \pm 2.168	32.15 \pm 5.372	9.795 \pm 8.678
Unpaired Noisy	32.13 \pm 7.300	24.44 \pm 10.88	21.51 \pm 8.690

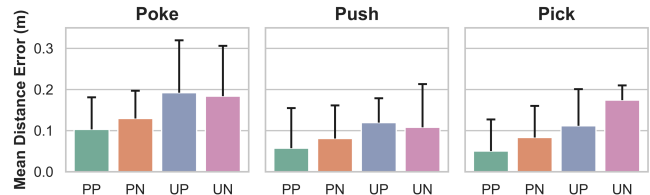


Fig. 6. Final object position error (mean + std) for the simulation experiment. Results are shown across the three tasks for models trained with our pairing algorithm on perfect (PP) and noisy (PN) datasets, and models trained with randomly paired data on perfect (UP) and noisy (UN) datasets.

For the simpler poke action, the *Noisy* dataset led to a statistically significant reduction in trajectory error (paired t-test, $p < 0.05$), while no significant difference was observed for the final object position (paired t-test, $p = 0.06$). For the push action, we found no statistically significant difference between the Perfect and Noisy conditions for either trajectory (paired t-test, $p = 0.76$) or object position error (paired t-test, $p = 0.14$). These findings indicate that while perfect demonstrations are advantageous for complex tasks, our algorithm enables the model to learn robust policies for simpler interactions even from imperfect data, achieving a performance level that is comparable to the perfect case.

b) *Comparison with Baselines*: Trajectory and object errors and success rates for the proposed method and the baselines are shown in Table III. Overall, the proposed method demonstrated a superior performance compared to the best-performing baseline **DP-Mode**, with statistical significance in all three metrics (paired t-tests, $p < 0.001$ each), despite having an order of magnitude fewer trainable weights. The results imply that the diffusion-based baselines had difficulty learning a generalizable representation of task parameters of novel objects (sphere and box) under the availability of paired and auxiliary task parameters.

c) *Extrapolation Capabilities*: A key result of this experiment is the model’s ability to extrapolate to objects that

TABLE III
RMSE FROM GROUND TRUTH TRAJECTORY AND DISTANCE ERROR (DE)
FOR FINAL OBJECT POSITION (MEAN \pm STD), AND SUCCESS RATES OUT
OF 10 TRIALS (MEAN) OVER 5 RUNS

Method	Traj. Error	Obj. Error	Success Rate		
	RMSE (deg)	DE (cm)	Poke	Push	Pick
Ours (UP)	26.21 \pm 13.18	14.12 \pm 10.18	0.0	0.0	3.4
DP-Dual	25.36 \pm 8.19	20.52 \pm 6.66	—	—	—
DP-2Head	16.46 \pm 8.66	20.56 \pm 6.67	—	—	—
DP-Mode	8.75 \pm 8.46	13.44 \pm 10.50	7.4	4.8	4.2
Ours (PP)	5.11 \pm 5.96	7.04 \pm 8.72	10.0	8.6	8.2

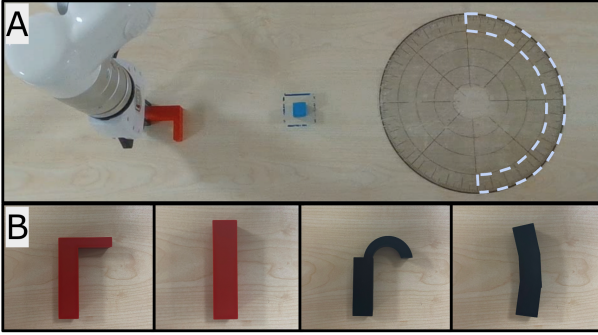


Fig. 7. The real robot experimental setup. (A) The tabletop environment, showing the xArm 7 robot, the cube’s initial position for the forward task (final position for the inverse task), and the highlighted area on the dial (possible final positions for the forward task). (B) The 3D-printed tools used: L-stick and Stick (red tools), and the novel Hook and Tilted-stick (black tool).

belong to the object classes presented in the Auxiliary dataset. The evaluation was conducted on a test set of spheres and boxes, which were entirely absent from the initial demonstration datasets ($\mathcal{D}^{\text{Perfect}}$ and $\mathcal{D}^{\text{Noisy}}$) that contained only cylinders. The model’s success on these novel objects was enabled by the auxiliary dataset (\mathcal{D}_{aux}), which provided examples of forward task executions for spheres and boxes. By leveraging these auxiliary demonstrations, the model successfully integrated the representations of the new objects into its latent space. Consequently, it was able to infer the correct corresponding behavior for the inverse task, such as applying a poking action to a sphere. The extrapolation in the pick modality is particularly noteworthy. Unlike the poke and push actions, which rely on a categorical distinction between objects, successful picking requires the model to regress the specific orientation of the novel boxes (visualized in bottom row of Figure 5). This successful inference of continuous geometric parameters for a complex manipulation skill provides compelling evidence that the model has formed a rich, structured latent representation of the new object classes.

C. Tool Extrapolation in Real Robot

To demonstrate the robustness of the proposed method against real-world conditions characterized by noisy sensor observations and imperfect actuation, we designed an experiment where a robot must learn to manipulate an object with novel tools. Unlike the simulation experiment, extrapolation is performed over a set of tools, and the task parameter includes the object position derived from downstream sensor observations, and all demonstrations are provided by a human operator. We also assessed the data efficiency of the method by comparing models trained with a full auxiliary set against a minimal one containing only two demonstrations.

1) *Experiment Setup*: In this experiment, a 7-DoF xArm 7 robotic arm equipped with a standard gripper is used, an Intel RealSense camera is mounted overhead to capture the workspace, and 4 different 3D-printed tools are utilized during the demonstrations, as shown in Figure 7.

We defined two tasks:

- **Forward Task - Push**: The robot uses a tool held in its gripper to push a blue cube from a fixed starting position

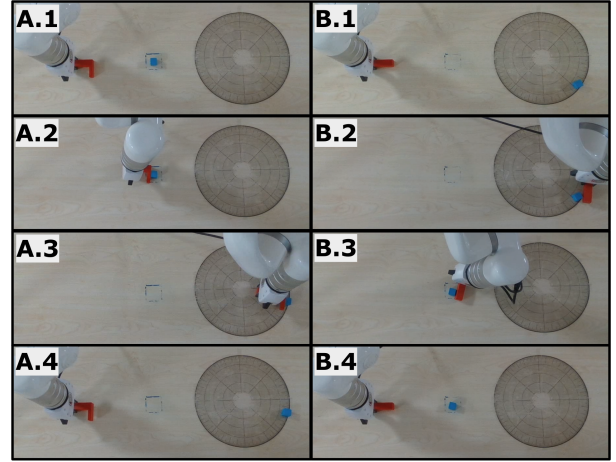


Fig. 8. Examples of the demonstrations in the real robot experiment. On the left (A.1-A.3), frames from the execution of the forward task (Push) using an L-stick, with the final environment shown in A.4. On the right (B.1-B.3), frames from the execution of the inverse task (Pull) using a Stick, with the final environment shown in (B.4).

to a target (x, y) coordinate within a designated area (highlighted in Figure 7.A) on a circular dial.

- **Inverse Task - Pull**: The robot uses the same tool to pull the cube from its position on the dial back to the initial starting position.

For each demonstration (examples shown in Figure 8), we recorded the joint angles of the robot as the sensorimotor trajectory, τ . The task parameter, ψ , was a vector consisting of the (x, y) coordinates of the blue cube and a feature vector derived from an RGB image of the tool. The coordinates are computed from the workspace image pixel values, and the tool images were preprocessed by segmenting the tool and extracting its edge contours to form feature vectors.

a) *Datasets*: The following dataset is demonstrated in the workspace:

- **Initial Sets ($\mathcal{D}_F, \mathcal{D}_I$)**: 40 demonstration pairs, including 20 with Stick and 20 with L-stick.
- **Auxiliary Set (\mathcal{D}_{aux})**: 20 Push demonstrations only, including 10 with a Tilted-stick and 10 with a Hook.

The state variables (S_{init} and S_{final}) was defined as the position of the object. The demonstrations in the initial dataset is then paired according to the final position of the object after forward demonstrations, and the initial position of the object before inverse demonstrations.

b) *Model*: The trained models employ MLPs as encoder and decoder layers, and a CNN to embed the task parameter. We trained the model under two conditions: training with the full Auxiliary set and with a minimal set (2 demonstrations, including 1 with a Tilted-stick and 1 with a Hook). The models (1.7M trainable weights) are trained with $p_{aux} = 0.25$, batch size 16 for 100K steps using AdamW optimizer (lr: $1 * 10^{-4}$, weight decay: $1 * 10^{-3}$). To evaluate the model, we placed the cube at 10 different points on the circular dial and generated 10 pull trajectories for each novel tool. We also demonstrated 20 trajectories for the inverse task with the Tilted-stick and Hook as ground-truth trajectories for further evaluation.

TABLE IV
RMSE FROM GROUND TRUTH (MEAN \pm STD) IN DEGREES.

	Full Auxiliary (20 D)	Minimal Auxiliary (2 D)
Tilted-stick	8.475 \pm 2.313	9.058 \pm 1.783
Hook	9.129 \pm 1.894	8.183 \pm 2.083
Total	8.802 \pm 2.139	8.621 \pm 1.987

D indicates the number of demonstrations.

2) *Results*: In this experiment, we consider an inverse demonstration successful if the robot manages to move the object from its position on the circular dial to the area surrounded by blue lines (Figure 8.B). We used the model trained with the minimal Auxiliary set to generate trajectories. The robot successfully completed the pull task in **7 out of 10** trials for both novel tools, the tilted stick and the hook, illustrating that our approach can effectively learn a shared latent space and leverage it to generalize to novel task parameters.

We also computed the Root Mean Squared Error (RMSE) between generated trajectories and ground-truth demonstrations for both training conditions (full and minimal Auxiliary sets), as shown in Table IV. The model trained with the minimal Auxiliary set shows performance comparable to the model trained on the full Auxiliary set. Crucially, there is no statistically significant difference between the two conditions (paired t-test, $p = 0.72$), highlighting the remarkable data efficiency of our method. Furthermore, we analyzed the activations from the CNN used for tool image embedding. The novel Tilted-stick produced a similar embedding to the Stick tool (Full Aux.: 0.1024 vs. 0.4836; Min Aux.: 0.0001 vs. -0.3393), while the Hook tool is similar to the L-stick tool (Full Aux.: -0.0573 vs. -1.0096; Min Aux.: 2.2025 vs. 0.5187), suggesting that the network learns a semantically meaningful representation of tool geometry.

IV. CONCLUSION

We proposed a novel joint learning framework that enables generalization capabilities to novel task parameters by transferring knowledge between a jointly learned forward-inverse task pair. Through comprehensive experiments on synthetic, simulated, and real-world data, we showed that our demonstration-pairing algorithm is critical for establishing a coherent common latent space, and that our architectural extensions and training methodology enable a robot to efficiently transfer knowledge and extrapolate manipulation skills to novel task parameters, such as objects and tools. We also show that our method outperforms diffusion-based baselines in the simulation experiment. Our approach provides a data-efficient solution within imitation learning by leveraging the assumption that novel task parameters can be projected to known behaviors. A limitation of our framework is its foundational assumption that novel auxiliary task parameters can be mapped to known behaviors within the existing sensorimotor space of the forward-inverse task pair provided in the paired demonstrations. Although the presented method is confined to forward-inverse tasks where an intuitive state-based pairing algorithm is effective, the core principle can be extended to

any related task pair. This would likely require a more complex pairing algorithm capable of discovering the underlying structural relationship between tasks. Nevertheless, we believe this principle of transferring knowledge through a jointly learned latent space is a promising direction for developing more adaptable and generalizable robots.

REFERENCES

- [1] J. Tobin, R. Fong, A. Ray, J. Schneider, W. Zaremba, and P. Abbeel, "Domain randomization for transferring deep neural networks from simulation to the real world," in *2017 IEEE/RSJ IROS*, 2017, pp. 23–30.
- [2] F. Muratore, F. Ramos, G. Turk, W. Yu, M. Gienger, and J. Peters, "Robot learning from randomized simulations: A review," *Frontiers in Robotics and AI*, vol. Volume 9 - 2022, 2022.
- [3] E. Jang, A. Irpan, M. Khansari, D. Kappler, F. Ebert, C. Lynch, S. Levine, and C. Finn, "Bc-z: Zero-shot task generalization with robotic imitation learning," in *CORL*, 2022.
- [4] X. B. Peng, M. Andrychowicz, W. Zaremba, and P. Abbeel, "Sim-to-real transfer of robotic control with dynamics randomization," in *2018 IEEE ICRA*, 2018, pp. 3803–3810.
- [5] M. Andrychowicz, B. Baker, M. Chociej, R. Józefowicz, B. McGrew, J. Pachocki, A. Petron, M. Plappert, G. Powell, A. Ray, J. Schneider, S. Sidor, J. Tobin, P. Welinder, L. Weng, and W. Zaremba, "Learning dexterous in-hand manipulation," *IJRR*, vol. 39, pp. 3–20, 2020.
- [6] K. Pertsch, R. Desai, V. Kumar, F. Meier, J. J. Lim, D. Batra, and A. Rai, "Cross-domain transfer via semantic skill imitation," *CORL*, 2022.
- [7] H. Niu, J. Hu, G. Zhou, and X. Zhan, "A comprehensive survey of cross-domain policy transfer for embodied agents," in *IJCAI*, 2024.
- [8] A. J. Ijspeert, J. Nakanishi, H. Hoffmann, P. Pastor, and S. Schaal, "Dynamical movement primitives: Learning attractor models for motor behaviors," *Neural Computation*, vol. 25, no. 2, p. 328 – 373, 2013.
- [9] M. Saveriano, F. J. Abu-Dakka, A. Kramberger, and L. Peternel, "Dynamic movement primitives in robotics: A tutorial survey," *IJRR*, vol. 42, pp. 1133–1184, 2023.
- [10] A. Paraschos, C. Daniel, J. R. Peters, and G. Neumann, "Probabilistic movement primitives," in *NIPS*, 2013.
- [11] M. Y. Seker, M. Imre, J. Piater, and E. Ugur, "Conditional neural movement primitives," in *RSS*, 2019.
- [12] R. Pérez-Dattari and J. Kober, "Stable motion primitives via imitation and contrastive learning," *IEEE TRO*, vol. 39, pp. 3909–3928, 2023.
- [13] C. Chi, Z. Xu, S. Feng, E. Cousineau, Y. Du, B. Burchfiel, R. Tedrake, and S. Song, "Diffusion policy: Visuomotor policy learning via action diffusion," *The International Journal of Robotics Research*, 2024.
- [14] E. Chisari, N. Heppert, M. Argus, T. Welschehold, T. Brox, and A. Valada, "Learning robotic manipulation policies from point clouds with conditional flow matching," *CORL*, 2024.
- [15] Q. Zhang, Z. Liu, H. Fan, G. Liu, B. Zeng, and S. Liu, "Flowpolicy: Enabling fast and robust 3d flow-based policy via consistency flow matching for robot manipulation," in *AAAI*, 2025.
- [16] K. Nguyen, A. T. Le, T. Pham, M. Huber, J. Peters, and M. N. Vu, "Flowmp: Learning motion fields for robot planning with conditional flow matching," in *2025 IEEE/RSJ IROS*, 2025, pp. 11 291–11 297.
- [17] S. Ross, G. Gordon, and A. Bagnell, Drew, "Reduction of imitation learning and structured prediction to no-regret online learning," 2011.
- [18] H. Perez-Villeda, J. Piater, and M. Saveriano, "Learning and extrapolation of robotic skills using task-parameterized equation learner networks," *Robotics and Autonomous Systems*, vol. 160, p. 104309, 2023.
- [19] M. Garnelo, D. Rosenbaum, C. Maddison, T. Ramalho, D. Saxton, M. Shanahan, Y. W. Teh, D. Rezende, and S. A. Eslami, "Conditional neural processes," in *ICML*, 2018.
- [20] M. Y. Seker, A. Ahmetoglu, Y. Nagai, M. Asada, E. Oztop, and E. Ugur, "Imitation and mirror systems in robots through deep modality blending networks," *Neural Networks*, vol. 146, pp. 22–35, 2022.
- [21] M. Akbulut, E. Oztop, M. Y. Seker, H. X. A. Tekden, and E. Ugur, "Acnmp: Skill transfer and task extrapolation through learning from demonstration and reinforcement learning via representation sharing," in *CORL*, 2021.
- [22] H. Aktas, Y. Nagai, M. Asada, E. Oztop, and E. Ugur, "Correspondence learning between morphologically different robots via task demonstrations," *RA-L*, 2024.
- [23] E. Oztop, M. Kawato, and M. A. Arbib, "Mirror neurons: functions, mechanisms and models," *Neuroscience letters*, vol. 540, p. 43, 2013.
- [24] H. W. Kuhn, "The hungarian method for the assignment problem," *Naval Research Logistics Quarterly*, vol. 2, no. 1-2, pp. 83–97, 1955.

- [25] E. Todorov, T. Erez, and Y. Tassa, "Mujoco: A physics engine for model-based control," in *2012 IEEE/RSJ IROS*, 2012, pp. 5026–5033.
- [26] K. He, X. Zhang, S. Ren, and J. Sun, "Deep residual learning for image recognition," in *Proceedings of the IEEE CVPR*, 2016, pp. 770–778.
- [27] R. Cadene, S. Alibert, A. Soare, Q. Gallouedec, A. Zouitine, S. Palma, P. Kooijmans, M. Aractingi, M. Shukor, D. Aubakirova, M. Russi, F. Capuano, C. Pascal, J. Choghari, J. Moss, and T. Wolf, "Lerobot: State-of-the-art machine learning for real-world robotics in pytorch," <https://github.com/huggingface/lerobot>, 2024.